2D/3D covalent organic frameworks based on cobalt corroles for CO binding

J. Yang, L. André, N. Desbois, C.P. Gros, S. Brandès

2D/3D Covalent Organic Frameworks based on cobalt corroles for CO binding

Jian Yang, Laurie André,* Nicolas Desbois, Claude P. Gros* and Stéphane Brandès*

Institut de Chimie Moléculaire de l'Université de Bourgogne, ICMUB, UMR CNRS 6302, Université Bourgogne Franche-Comté, 9, Avenue Alain Savary, BP 47870, 21078 Dijon cedex, France.

ABSTRACT

In the present work, the synthesis, characterization and gas adsorption properties of new 2D COF (**2D-COF-Cor**) and 3D COF (**3D-COF-Cor**) based on corrole macrocycles are reported. The two COFs have been synthesized by Schiff base condensation from readily available C_3-symmetric aldehyde or T_d-symmetric aldehyde as platforms, and diamine-functionalized free-base corrole as building block linker, to access 2D and 3D polymers respectively. Cobalt metalated COFs were also synthesized using a post-metalation procedure, to give **2D-COF-CorCo** and **3D-COF-CorCo** as porous materials. The designs of the 2D and 3D structures of the materials are reported, as well as the relationship between their structure and their performances for carbon monoxide (CO) adsorption. Spectroscopy analyses such as ^{1}H NMR, FTIR, powder X-ray diffraction, microscopic analyses, and sorption measurements were used to fully characterize the structure and the porosity of the COF materials. Their properties for capture and sensing of CO were also studied with the analysis of their isotherms using a multisite Langmuir isotherm model and the IAST theory. The affinity, capacity and selectivity of these materials for CO sorption were calculated. Compared to **3D-COF-CorCo**, **2D-COF-CorCo** reveals the highest adsorption capacity of 32.2 $cm^3\,g^{-1}$ for CO (298 K, 1 atm) with a high selectivity over N_2, O_2, CO_2, up to 50130, 5090, 3170, respectively. In addition, FTIR analysis gave clear evidence of the involved solid-gas interactions, and the reversibility, of CO binding on the cobalt metal center of the corrole within the materials. These results point out an appealing way of using cobalt corrole-based COF as efficient chemosensors to detect trace amounts of CO.

Keywords: 2D COF, 3D COF, porphyrinoids, corroles, cobalt corroles, CO binding, gas adsorption

*Corresponding authors.
E-mail address: laurie.andre@u-bourgogne.fr (L. André), Claude.Gros@u-bourgogne.fr (C. P. Gros) and Stephane.Brandes@u-bourgogne.fr (S. Brandès)

ORCID

Laurie André: 0000-0002-9574-9617

Nicolas Desbois: 0000-0002-1156-4608

Claude P. Gros: 0000-0002-6966-947X

Stéphane Brandès: 0000-0001-6923-1630

1. Introduction

Carbon monoxide (CO) poisoning is the most common form of fatal poisoning in many countries [1]. This colorless, odorless and harmful gas [2, 3], is one of the most common and widely distributed air pollutant [4]. Most commercial CO detectors are based on electrochemical cells or metal-oxide semiconductors [5]. Metal-oxide semiconductors such as SnO_2 [6], ZnO [7], In_2O_3[8], TiO_2 [9], CeO_2 [10], Fe_2O_3 [11], WO_3 [12], CdO [13], CuO [14], composite oxides [15], and yttria-stabilized zirconia (YSZ) [16] have been described for CO sensing. However, metal-oxide semiconductors and electrochemical sensors present the main issue of requiring high operating temperature. In addition, due to gaseous interferences like nitric oxide (NO), ammonia (NH_3), hydrogen sulfide (H_2S), and humidity (H_2O), these electrochemical and metal-oxide semiconductor sensors also suffer from relatively poor selectivity [17-19]. Therefore, it is worthwhile to develop new materials with high performances for CO sensing.

Cobalt corroles could play a key role for the synthesis of new CO sensing materials [20-23]. Corrole is an important class of tetrapyrrolic macrocycles that possesses an 18 π-electron conjugated system. Compared to porphyrin, corroles present a direct pyrrole–pyrrole link instead of one *meso*-carbon [24, 25]. The contracted porphyrin structure leads to a smaller macrocyclic core size of the corrole and unique coordination abilities of metal ions due to the trianionic character of the macrocycle, which helps to stabilize metal ions in higher oxidation states compared to porphyrin analogs [26-28]. We have previously reported that cobalt metallocorroles are able to bind CO on the cobalt(III) center, and without any interference from dioxygen (O_2), nitrogen (N_2), and carbon dioxide (CO_2) due to, advantageously, no coordination of these interferent gases on the cobalt center [20, 22, 29].

However, despite their high selectivity for CO, the number of active sites of cobalt corrole for gas binding is far from optimal in the solid state. A stable and highly porous material that combines cobalt corroles and structurally rigid building blocks could efficiently improve the CO adsorption capacity. Thanks to a better accessibility of the cobalt center for gas binding, the adsorption kinetic could be improved and fast saturation of the sensor could be avoided. Recently, Porous Organic Polymers (POP) based on cobalt corrole were reported by our group and their good affinities of CO adsorption were shown to be promising for the further design of new CO sensors [22].

Unlike POP, COF is a unique class of porous organic materials which possesses many advantages such as low mass density [30, 31], high surface area [2, 32], permanent porosity

[33, 34], high thermal stability [35, 36], and can also present good crystallinity thanks to the reversible assembly reactions of the building blocks [37, 38]. COFs have gained significant attention in the past decade due to their widespread application in gas adsorption and separation [39, 40], catalysis [41, 42], sensors [43, 44], optoelectronic devices [45, 46] and clean energy [47, 48]. However, no COF has been used to capture or detect carbon monoxide so far. On the molecular level, COFs allow the integration of building blocks and adjustment of the resulting materials with well-defined structure and symmetry, to reach out the pre-designed composition, topology and porosity [33, 49]. Depending on the geometry and connectivity of the precursors, COFs can develop into two-dimensional layered structures (2D COFs) or three-dimensional extended networks (3D COFs) [50]. The layered structures of 2D COFs result in the formation of periodically ordered columnar π-arrays and aligned one-dimensional nanochannels in an AA or ABA packing fashion, and can be used for separation of small molecules [51, 52]. In contrast, the organization of the building blocks in 3D COFs allows the structure to extend in the three-dimensional space suggesting a highly open porosity and a good accessibility of the active sites [53].

In addition, the interactions between the functional monomers inside of the 2D and 3D COFs present key differences influencing the properties of the resulting materials, including pore sizes, shapes and distribution [54, 55]. Thus, for comparison purposes, we built 2D and 3D COFs with a corrole bearing the same moiety, and we have investigated the effect of dimensionality on their properties including porosity, surface area, and propensity for the selective adsorption of different gas molecules [56-59]. Until now, only two COFs based on the corrole macrocycle were reported by Zhang's group [27], and Ma's group [60]. The reported two COFs were formed thanks to the Schiff base condensation between a tri-amino corrole and a bis-aldehyde derivative. Both of them feature good porosities, stabilities and crystallinities. These two COFs based on corrole were used for potential application in photodynamic therapy and in metal chemosensing, respectively.

Since we already reported that cobalt corroles are sensitive and selective to carbon monoxide (CO) [21, 22], their insertion into the porous structures of COFs can be a way to achieve highly sensitive and selective CO sensing. Therefore, the main goal that we pursue is to develop new COFs based on cobalt corrole for a highly sensitive and selective CO adsorption while retaining the framework permanent porosity.

Several reversible reactions such as Schiff base reaction, spiro-borane condensation, Knoevenagel condensation, and imide condensation were successfully employed for the construction of crystalline COFs [61]. In particular, imine-based COFs have gained great

attention and have become, during the last few years, one of the most popular backbones in this field [62]. Such interest is well deserved because of the suitable thermal, water, and chemical stability of COFs prepared by Schiff base reaction [63] when they are used in non-drastic conditions. In addition, these synthetic procedures often gave high yield, versatility of their functional amine- and aldehyde-bearing precursors [64], mild reaction conditions, and easily available catalysts [52].

The two 2D and 3D COF of our interest are based on hexagonal honeycomb-like and diamond-like topologies respectively. Thanks to the design of reticular chemistry, monomers possessing the appropriate size and symmetry can be chosen to construct porous 2D or 3D COFs with such topologies and high reticulation. With these approaches, for the first time, corrole plays a role as C_2 symmetric linker with two reacting functional groups. We report herein the targeted synthesis of a 2D COF and its 3D COF analog, assigned as **2D-COF-Cor** and **3D-COF-Cor**, respectively, starting from near C_2 symmetric 5,15-bis(4-aminophenyl)-10-(4-trifluoromethylphenyl)corrole and C_3 symmetric 1,3,5-triformylbenzene or T_d symmetric tetrakis(4-formylphenyl)methane through the [3+2] and [4+2] imine condensation reaction.

2. Results and discussion

2.1.Synthesis of the materials

The preparation of 2D and 3D corrole based COFs described in Scheme 1 requires to synthesize a bis-aminocorrole monomer (**corrole-NH_2**, see SI for experimental details and characterizations). The corrole macrocycle was obtained by cyclisation of an aryl aldehyde with 5-(4-nitrophenyl)dipyrromethane the latter being prepared pure with high yield using $MgBr_2$ as catalyst according to a reported procedure [65]. The *meso*-substituted *trans*-A_2B-corrole is accessible *via* a classical [2+1] approach from the above dipyrromethane and 4-(trifluoromethyl)benzaldehyde in a MeOH/H_2O mixture. Finally, the dinitrocorrole was converted into its diamino analog with 85 % yield by reduction under 1 atm of H_2 using Pd/C as catalyst. The tetrakis(4-formylphenyl)methane platform was prepared according to the described procedures (see Section 2 in the SI) and the 1,3,5-triformylbenzene platform was purchased. Among the possible synthetic strategies to obtain COFs (solvothermal, microwave, ionothermal, mechanochemical…), we have focused our work on the solvothermal method due the convenience and ease of application. In order to obtain a 2D COF, the control of the topology of the resulting material was addressed by using planar C_3 symmetric building block acting as node of the framework. We have then chosen 1,3,5-triformylbenzene to react with C_2

symmetric **corrole-NH$_2$** according to an [2+3] imine condensation. The COF was prepared by reaction of stoichiometric amount of both reagents in a mixed solution of *n*-butanol, mesitylene and 6 M aqueous acetic acid (Scheme 1) and a dark green powder identified as **2D-COF-Cor** was obtained after 3 days at 120 °C. The synthesis of a corrole-based 3D COF was also attempted. Up to now, the largest number of 3D COFs have been developed by assembling C_2 and T_d symmetric building blocks, which yields diamond-like topology networks [55, 66]. To obtain a 3D COF based on **corrole-NH$_2$** thanks to a [2+4] imine condensation, we were inspired by porphyrin-based COFs that were prepared from a T_d node like tetrakis(4-formylphenyl)methane [50, 67, 68]. Hence, the **3D-COF-Cor** was synthesized starting from **corrole-NH$_2$** and tetrakis(4-formylphenyl)methane in a mixed solution of *n*-butanol, *o*-DCB and 6 M aqueous acetic acid (Scheme 1).

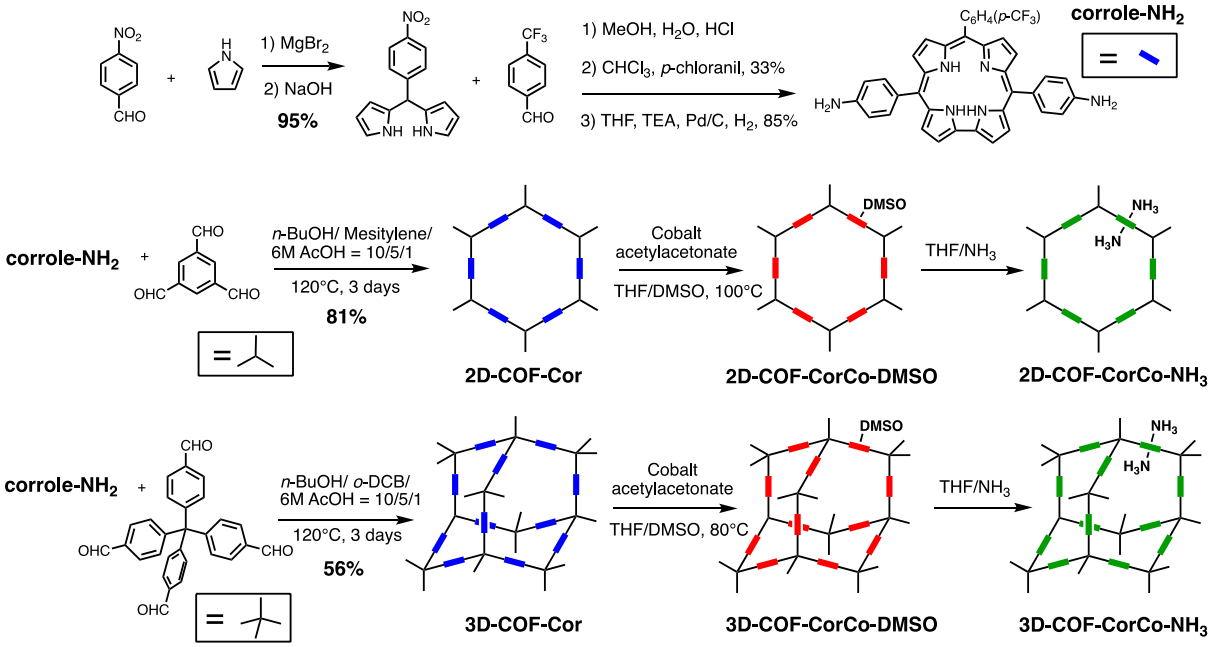

Scheme 1. Synthetic route of **2D-COF-Cor**, **3D-COF-Cor** and their cobalt complexes.

The desired COFs containing cobalt complexes were obtained *via* the metalation of the free base corroles in the synthesized **2D-COF-Cor** and **3D-COF-Cor**. Each COF was suspended in a solution of cobalt acetylacetonate dissolved in a mixture of DMSO and THF. For **2D-COF-Cor**, the solutions were then heated without magnetic stirring for 5 h at 100 °C. Meanwhile, the reaction mixture with **3D-COF-Cor** was treated similarly, but it was heated at only 80 °C as lower temperature proved sufficient to complete the metalation with a high yield. This difference was assumed to be due to the π-electron rich structure of the corrole and the AA-π-stacking of the **2D-COF-Cor** making the insertion of the cobalt in the corrole of the 2D-COF

more difficult than it is in the 3D-COF analog. According to this protocol, we obtained the two COFs containing the cobalt corrole complexes, **2D-COF-CorCo-DMSO** and **3D-COF-CorCo-DMSO** with one single DMSO axial ligand on the cobalt (see elementary analyses in the Supporting Information). Indeed, our group had previously reported that cobalt corroles with a single DMSO or two NH_3 ligands on the cobalt center are stable in air [69]. However, the NH_3 ligands on the cobalt corrole complex can be easily removed under vacuum at 80 °C, while it is much more difficult to remove the DMSO ligand. For this reason, the DMSO was exchanged for NH_3 by washing the materials with a solution of THF saturated with ammonia to afford **2D-COF-CorCo-NH_3** and **3D-COF-CorCo-NH_3** coordinated by two NH_3 ligand on the cobalt center. Before CO binding tests, the NH_3 ligands were removed and the quantity of cobalt in the 2D and 3D COF was determined by ICP. For **2D-COF-CorCo**, the ICP analysis gives a 5.88 %wt of Co (0.099 mmol g^{-1}) against 7.45 %wt for the theoretical value. For **3D-COF-CorCo**, we obtain 4.59 %wt for Co (0.078 mmol g^{-1}), against a theoretical value of 6.25 %wt.

2.2.Material characteristics

The **2D-COF-Cor** and **3D-COF-Cor** clearly exhibit the formation of networks linked by C=N bonds that give a typical C=N stretching vibration at about 1610 cm^{-1} [27, 60]. Indeed, the comparison of the IR spectra for the starting compounds 1,3,5-triformylbenzene and **corrole-NH_2** clearly shows the formation of the imine bond by the vibration at 1614 cm^{-1} for **2D-COF-Cor** (Fig. 1a). However, a peak at 1699 cm^{-1} attests to the presence of the terminal aldehyde groups in the resulting material, while the consumption of the amino groups, evidenced by the absence of the NH vibration around 3460 cm^{-1} is nearly complete. The sharp peak at 1323 cm^{-1} was tentatively assigned to the C–N stretching of the aromatic amine (Ph-N) groups which become bigger by the formation of conjugated imine linkages. The peaks at 1167 and 1128 cm^{-1} can be assigned to the C–N stretching of the azomethine (C-C=N-C) groups [52]. All of these results further support the formation of the imine networks and the IR spectrum of **3D-COF-Cor** is very similar to that of **2D-COF-Cor** (Fig. S18).

We also compared the FTIR spectra of COFs-Cor and their corresponding cobalt complex counterparts (Fig. 1b). After the cobalt metalation of the corroles within **2D-COF-Cor**, the characteristic peaks of **2D-COF-CorCo-DMSO** and **2D-COF-CorCo-NH_3** still match with that of the **2D-COF-Cor**. The metalated 2D-COFs still clearly show the imine bond around 1614 cm^{-1} and the peaks in the range of 3500-2800 cm^{-1} remain similar. Interestingly, for **COF-**

CorCo-DMSO (Fig. 1b and S19), a weak peak around 1014 cm^{-1} was more prominent and can be assigned to the S=O stretching from the DMSO ligands [70].

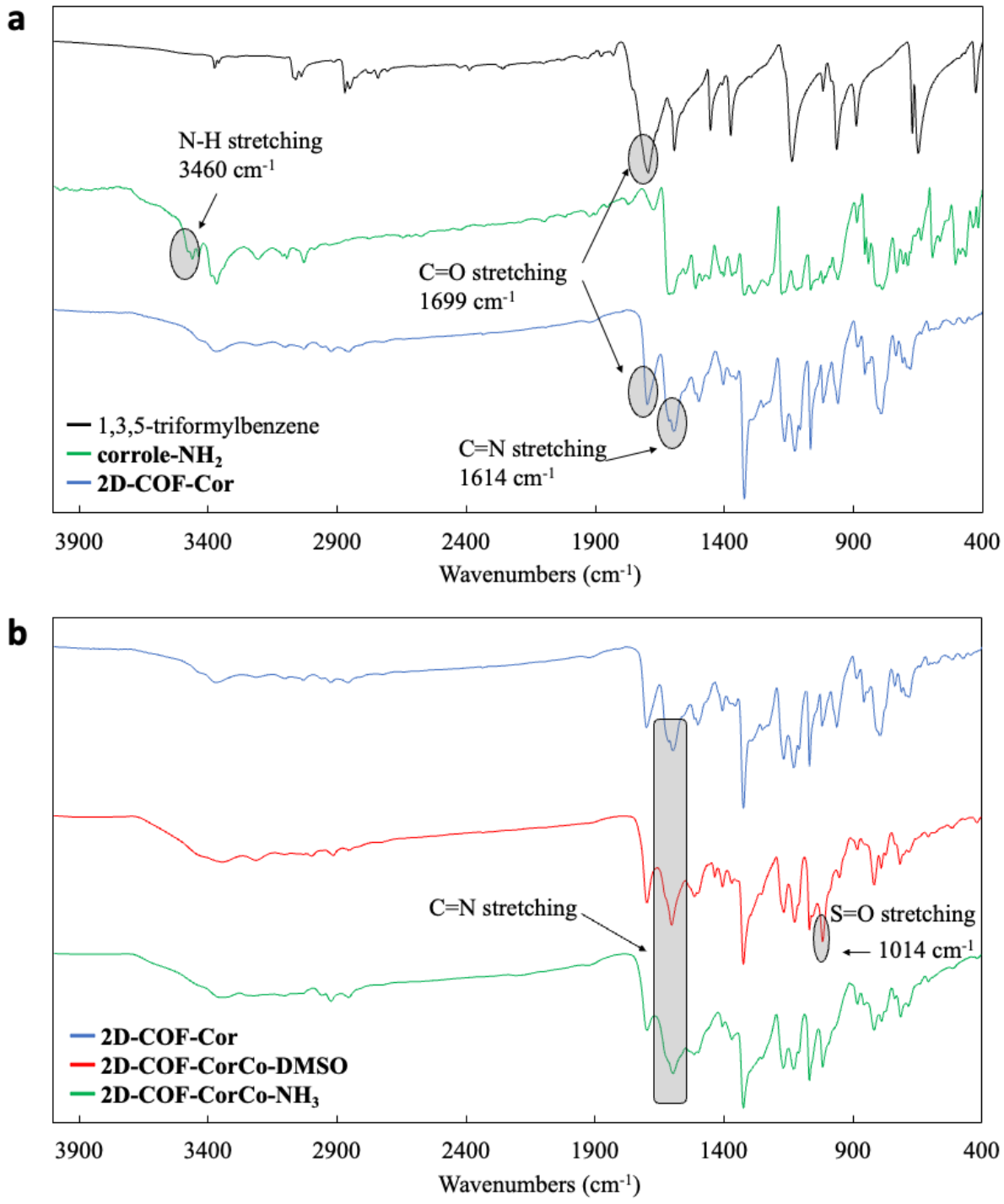

Fig. 1. a) FTIR spectra of 1,3,5-triformylbenzene, **corrole-NH_2** and **2D-COF-Cor**. b) FTIR spectra of **2D-COF-Cor**, **2D-COF-CorCo-DMSO** and **2D-COF-CorCo-NH_3**.

When NH_3 is coordinated to the cobalt center in the ligand, the peak at 3349 cm^{-1} (Fig. S20-S21) clearly showed the N-H vibration for **2D-COF-CorCo-NH3**. For **3D-COF-CorCo-NH3**, the similar N-H vibration appeared at 3352 cm^{-1}. During the FTIR analysis of **2D-COF-CorCo-NH3** and **3D-COF-CorCo-NH3**, a release of NH_3 ligand was observed due to the high vacuum inside the IR apparatus.

The integrity and the ratio of the building blocks in COFs were further confirmed by ^1H NMR analysis. Few milligrams of a suspension of polymers in deuterated dimethyl sulfoxide (DMSO-d_6) was decomposed after adding deuterium chloride (DCl) which hydrolyzes the imine functions and releases the starting amino and aldehyde derivatives. Finally, one drop of hydrazine ($N_2H_4 \cdot H_2O$) was added in order to reduce the traces of any corrole radical cations that usually impeded the good resolution of the ^1H NMR spectrum. For **2D-COF-Cor** shown in Fig. 2, all peaks are assigned to the amino-corrole and 1,3,5-triformylbenzene by comparing to the spectra of the starting compounds (Fig. S10). The signals at 8.77, 8.58, 8.39 and 8.12 ppm correspond to the β-pyrrolic protons of the corrole, and the aryl protons of the C_6H_4-CF_3 fragment are located at 8.23 and 8.01 ppm. The two more shielded doublets at 7.87 and 6.99 ppm correspond to the protons on the 5-*meso*- and 15-*meso*-phenyl rings. The signals of the aryl platform appear at 7.42 and 7.68 ppm and no aldehyde function was observed. It turns out that the hydrazide form of 1,3,5-trisformylbenzene was obtained after the reaction with hydrazine, and only the $CH{=}NNH_2$ function can be seen at 7.68 ppm. An average ratio of 1.1 corrole for 1 platform was determined by integration of the signals for **2D-COF-Cor**, which is quite close to the theoretical stochiometric ratio of 1.5 corrole for 1 platform. Since the imine formation is a reversible reaction, it is acceptable that a part of the corroles is lacking, which means that the material presents some corrole defects.

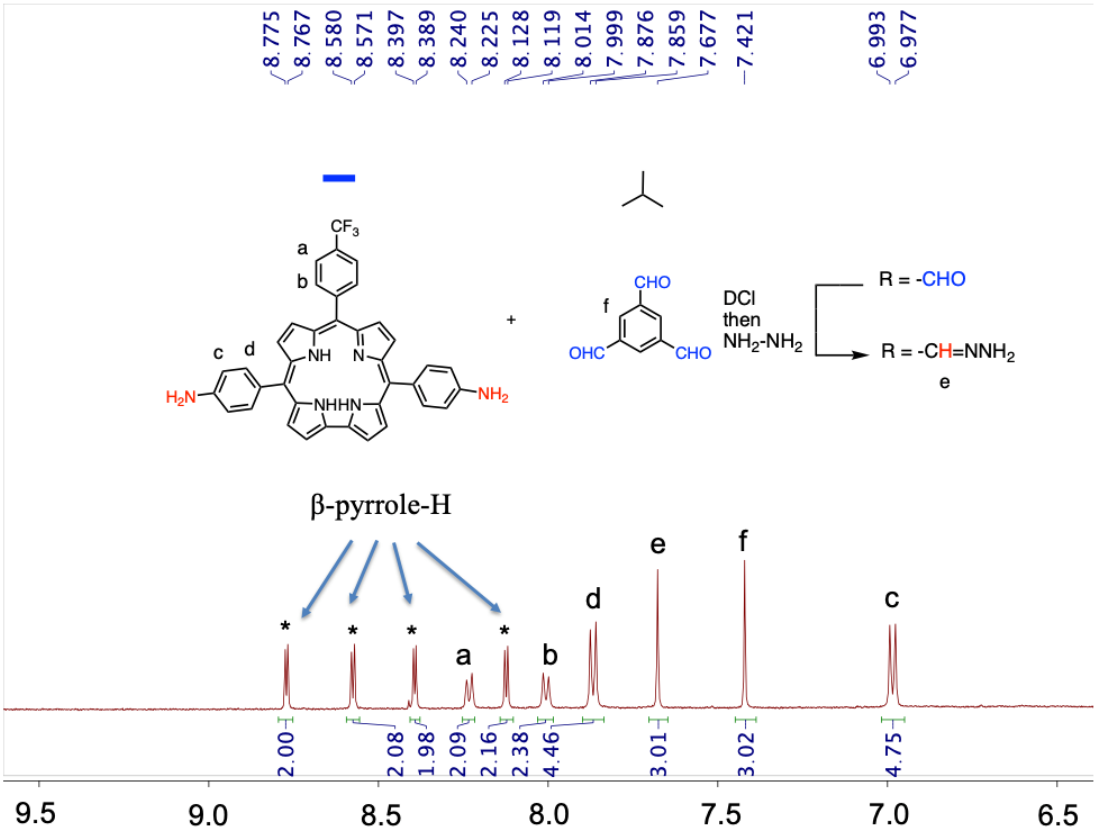

Fig. 2. ^{1}H NMR spectrum of **2D-COF-Cor** decomposed by DMSO-d_6/DCl (+50 µL hydrazine).

Concerning the 3D COF, the same ^{1}H NMR analysis was carried out (Fig. S17) and a similar ratio (1.1 corrole : 1 platform) was found, compared to a 2 : 1 ratio that is theoretically expected for a stochiometric defect-free material. Furthermore, the ^{1}H NMR spectra clearly showed there are no side products formed during the COF synthesis, which means that there is no degradation of corrole-NH_2. The results proved that the COFs structure helps to stabilize the corrole. The corrole to platform ratio calculated for both materials clearly show that the 2D COF likely present less-defect structure compared to its 3D counterpart.

PXRD analysis was also employed to determine the crystallinity of the synthesized COFs. As expected for a 2D COF, **2D-COF-Cor** showed a good crystallinity [71, 72]. The experimental PXRD pattern displayed in Fig. 3a shows three intense peaks at 2θ = 2.37°, 4.75° and 6.47° and a broad and weak peak at 24.5°, which are assigned to the (100), (200), (210) and (001) lattice planes respectively, indicating long-range order in this framework. By comparison with already described 2D COFs, the morphology of the experimental patterns suggests that the **2D-COF-Cor** is formed thanks to the eclipsed AA stacking mode [71, 72]. The unit cell parameters were determined as a = b = 43.0 Å, considering the crystal structure as a hexagonal packing. In addition, the broad signal at 24.5° indicates a layer spacing between two adjacent corroles

around 3.6 Å, which should be enough to allow the post-metallation of the COF with cobalt. This evidences that the macrocycles are still accessible despite their π–π stacking in the network. The crystallinity of the metalated COF **2D-COF-CorCo** was also investigated and it shows two main peaks at 2θ = 2.46° and 4.81° (Fig. S22). This result indicates that after inserting cobalt into the corrole macrocycles, **2D-COF-CorCo** retains the same topology but a slight shrinking of the lattice parameters was observed. For **3D-COF-Cor**, the PXRD indicates the amorphous nature of the material since we can observe no distinct diffraction features (Fig. S23). We assumed that the non-C_2 symmetric structure of corrole makes it very difficult to form well-organized diamond-like 3D structure for **3D-COF-Cor**. According to the literature, the 3D COF based on bifunctional C_2 symmetric porphyrin also shows no crystallinity [73]. In addition, the higher crystallinity observed for **2D-COF-Cor** indicates it is easier to form a well-organized structure for 2D materials, due to its topology itself and by the fact that **3D-COF-Cor** has more defects than its 2D analogue.

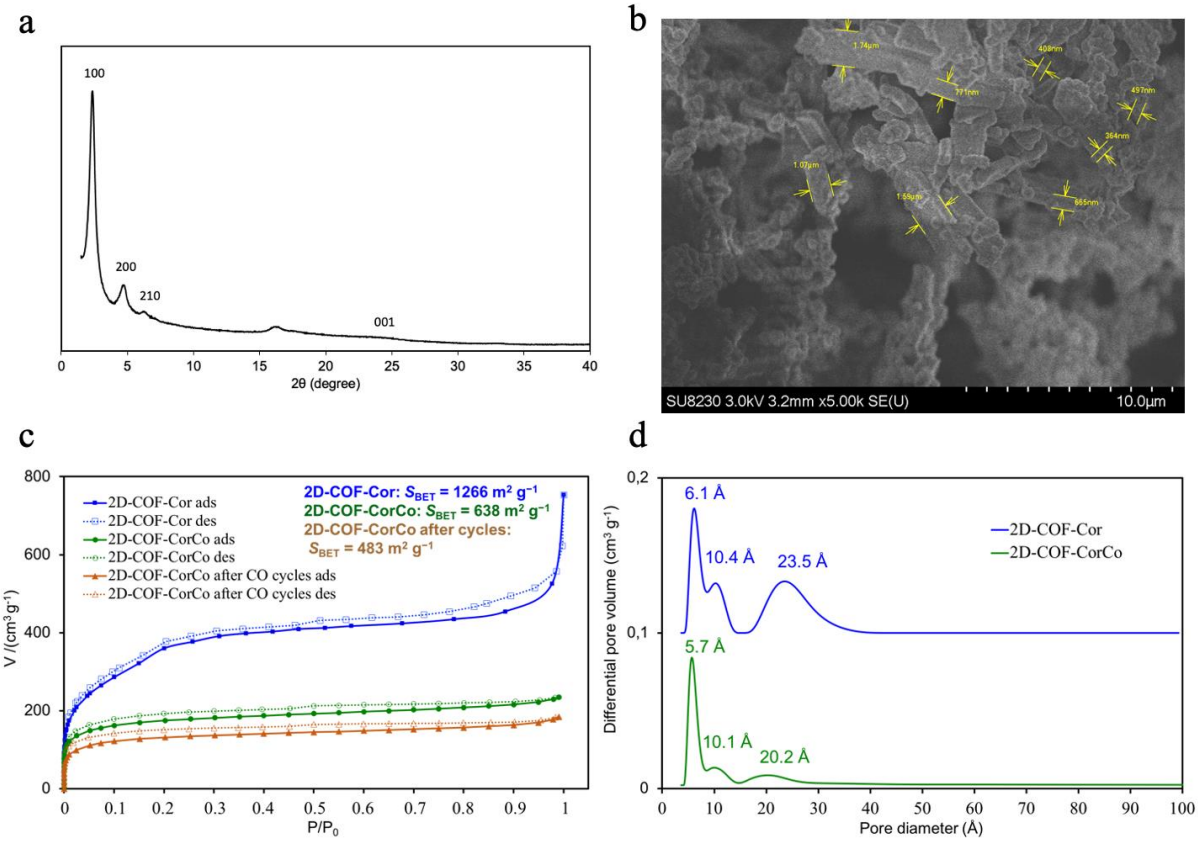

Fig. 3. a) PXRD patterns of **2D-COF-Cor**. b) SEM images of **2D-COF-Cor.** c) N_2 adsorption (closed symbols) and desorption (open symbols) isotherms recorded at 77 K for **2D-COF-Cor** (blue square), **2D-COF-CorCo** (green square), **2D-COF-CorCo** after CO cycles (brown square). d) The respective pore size distribution curves of **2D-COF-Cor** and **2D-COF-CorCo** calculated using the NLDFT method.

The macroscopic morphology of the free base COFs (**2D-COF-Cor** and **3D-COF-Cor**) and their corresponding metalated COFs (**2D-COF-CorCo-DMSO** and **3D-COF-CorCo-DMSO**) have been examined by Scanning Electron Microscopy (SEM) coupled with Energy Dispersive X-ray Spectrometry (EDS). Regular plate-shaped particles with a narrow thickness in the range 400-800 nm, but also of 1.0-1.5 μm length, were revealed (Fig. 3b and Fig. S24) for both **2D-COF-Cor**. Aside from those plate-shaped particles, granular crystallites bearing a sphere-like morphology are also present. Interestingly, the morphology and particle size remain similar after the insertion of cobalt into the corrole core (Fig. S24b). For **3D-COF-Cor** and **3D-COF-CorCo-DMSO**, a mixture of sphere-like and small plate-like particles were observed (Fig. S24a,c). We can assume that the smallest particles tend to form spherical aggregates around the size of 1.5-2.0 μm, which are favored under the solvothermal conditions. This may be the reason why there are two different shapes of particles co-existing in **3D-COF-Cor** and **3D-COF-CorCo-DMSO**.

The metalation ratios of 2D and 3D COF were calculated as 78 % and 72 % respectively, according to the percentage of corroles which is determined by ^{1}H NMR and ICP. For all COFs before and after metalation the presence of the fluorine present from the corrole macrocycle were confirmed by EDS analysis (Fig. S25-S28 and Tables S1-S4). For **2D-COF-CorCo-DMSO** and **3D-COF-CorCo-DMSO**, the presence of the Co and S elements attest of the cobalt metalated corroles and the coordinated DMSO on the cobalt complex. For 2D-COF-CorCo, the calculated average atomic ratio for Co/F from the EDS analysis is 0.22, while the expected ratio according to ICP is 0.26, giving evidence that corroles are more than half-metalated (Fig. S27, Table S1-S2). The same calculation was carried out for **3D-COF-CorCo**, and the average atomic ratio for Co/F is 0.19 against 0.24 for the expected ratio (Fig. S28, Table S3-S4). Due to the experimental errors related to each of the analysis techniques, we considered that the metalation ratio calculated from EDS and ICP are concordant.

Thermal stability of the COFs materials was investigated by thermogravimetric analyses (TGA) conducted in the range of 20 °C to 900 °C with a heating rate of 10 °C min^{-1} under a synthetic air gas flow (Fig. S29). The TGA curves for these COFs materials exhibited almost no weight loss between 200 °C and 300 °C and only **3D-COF-CorCo** and **2D-COF-Cor** showed a ~3 % weight loss due to water adsorption by the porosity of the materials. A second step was clearly observed due to the calcination of the organic part of the materials that occurs in a higher temperature range. The calcination temperature was similar for both COFS, as it was observed

in the range of 300 – 650 °C for **2D-COF-Cor** and **3D-COF-Cor**, and a shorter range of 300 – 460 °C was recorded for their metalated analogues. This result is clearly assigned to the destabilization of the corrole complexes compared to their respective free base. A plateau for **2D-COF-CorCo** and **3D-COF-CorCo** was reached at 9.0 % and 7.3 % respectively, and these values are in good agreement with the expected amount of cobalt(III) oxide (calcd for Co_2O_3: 8.3 % and 6.5 % according to ICP results). It is worthy of note that, when considering the corroles as fully metalated, the expected theoretical amount of cobalt(III) oxide were calculated as 10.5 % and 8.8 %. From the TGA analyses, we then calculate the metalation ratios to be about 86 % and 83 % for 2D and 3D COF respectively, which is close to the EDS and ICP results. Interestingly, the similarity of the thermograms between the free base COF in one hand and the metalated materials in the other hand clearly attests that despite their different topology, the 2D-COF and 3D-COF present the same stability. This result demonstrates that the thermal stability is dominated by both the nature of the linkages that connect corroles and platforms, by the nature of the corrole itself, and that neither the crystallinity nor the topology of the framework are preponderant for the control of the thermal stability.

In order to analyze the permanent porosity of COFs, nitrogen adsorption-desorption measurements were carried out at 77 K for the four materials. Before gas adsorption measurements, all the COFs were heated under vacuum at 80 °C for at least 3 h until the pressure reached 5×10^{-5} atm, making sure no solvent remained in the porous structure. **2D** and **3D-COF-Cor** both displayed nearly reversible type-I sorption behaviors (Fig. 3c and Fig. S30a). For the 2D COF, the sorption curves showed high nitrogen uptake at low relative pressure ($P/P_0 < 0.2$), which is a significant feature of microporous materials presenting also small mesopores of ~2 nm. The isotherm of **3D-COF-Cor** exhibits a typical type-I morphology with reversible desorption step. In addition, the high uptake in the higher-pressure range ($P/P_0 > 0.95$) is characteristic of intergranular sorption due to the presence of voids between the particles. After optimization of the COF synthesis with different reaction solvent systems and ratios, the highest BET surface area of **2D-COF-Cor** and **3D-COF-Cor** were obtained using the mixture *n*-BuOH/mesitylene/acetic acid (10:5:1, v/v/v) (Table S5) and mixture *n*-BuOH/*o*-DCB/acetic acid (10:5:1, v/v/v) (Table S6) respectively. The BET model was applied to the isotherm of **2D-COF-Cor** and **3D-COF-Cor** following the Rouquerol recommendations [74] to afford a BET surface area of 1141 $m^2 g^{-1}$ and 489 $m^2 g^{-1}$, respectively. Further studies were conducted on **2D** and **3D-COF-Cor** produced from large scale synthesis, and each sample exhibited a BET surface area of 1266 $m^2 g^{-1}$ and 484 $m^2 g^{-1}$ respectively, which corresponds to

the best optimization results and show the good reproducibility of the material synthesis. In the literature, the two reported COFs based on another free base corrole present a lower porosity [27, 60] around 745 and 634 $m^2 g^{-1}$ compared to 1266 $m^2 g^{-1}$ for the **2D-COF-Cor**, first described in the present study. Our team [22] and others [75] also recently described a 3D POP based on corrole which gave a values of 645 and 416 $m^2 g^{-1}$ compared to 484 $m^2 g^{-1}$ for our 3D COF. The study of the metalated **2D** and **3D-COF-CorCo** also revealed a typical type-I isotherm with a sharp uptake at relative low pressure ($P/P_0 < 0.1$), confirming their permanent porosity and the presence of microporosity with almost no mesoporosity, in contrary to the non-metalated materials. The BET surface areas were calculated to 638 and 489 $m^2 g^{-1}$, respectively. After metalation, the BET surface area of **2D-COF-CorCo** displayed a sharp decrease due to the stacking of 2D layers and some shrinking of the framework, as previously revealed by PXRD analyses. These structural and porosity changes were triggered by the insertion of cobalt into the corrole. NonLocal Density Functional Theory (NLDFT) fitting of the adsorption branch for **2D-COF-Cor** and **3D-COF-Cor** displays pore size distributions with average pore widths of 6.1 Å, 10.4 Å, 23.5 Å and 5.7 Å, 11.6 Å, 25 Å, respectively (see *e.g.* Fig. 3d and Fig. S30). This reveals the presence of micropores and small mesopores, as well as irregularities, in their structures but the mesoporous contribution is low for the 3D COFs, and it tends to vanish for the 2D COFs after metalation. Furthermore, the BET surface area of **2D** and **3D-COF-CorCo** after CO adsorption cycles showed a slight decrease compared to those before the CO adsorption cycles.

The CO adsorption properties of **2D-COF-CorCo** and **3D-COF-CorCo** were also evaluated along with the selectivity for CO *vs.* N_2, O_2 and CO_2, which are the main components of the air, and also the main potential interferents. As displayed in Fig. 4a,b, the adsorption isotherms for the gases were recorded at 298 K showing different adsorption volumes at 1 atm. At first glance, the results indicate a good capacity and selectivity for CO adsorption for both types of COFs. At 1 atm, the two materials display a CO uptake of 32.2 $cm^3 g^{-1}$ and 20.5 $cm^3 g^{-1}$ at 298 K, respectively. Most importantly, for CO adsorption, both materials displayed a sharp uptake at a very low pressure (< 0.01 atm) which is dominated by the binding of CO molecules on the cobalt in the corrole through a chemisorption process. After saturation of all the accessible cobalt sites by CO molecules, the rest of the adsorption process was then led by physisorption due to the porosity of the materials. **2D** and **3D-COF-CorCo** also exhibit adsorption for N_2, O_2 and CO_2 but only through physisorption, and no chemisorption was observed since no interaction occurred between these gases and cobalt corrole [20, 22]. Among these gases, a high

uptake of CO_2 at 1 atm occurred through a physisorption process due to the stronger interactions between the surface of the materials and CO_2.

Up to now and so far to our knowledge, our team is the only one that has reported porous materials based on cobalt corrole with a high affinity for CO at very low partial pressure [22], which is a prerequisite to provide a good selectivity in gas mixture containing a low concentration of CO. In order to describe the CO adsorption process, the isotherm data were fitted with a triple-site Langmuir model while a single-site Langmuir model enabled the fitting of the CO_2, N_2 and O_2 adsorption isotherms. The half saturation pressure for the selective sorption process is estimated to 0.65 10^{-4} atm and 0.46 10^{-4} atm for **2D-COF-CorCo** and **3D-COF-CorCo**, respectively. The two first components of the triple-site Langmuir model were assigned to the chemisorption of CO to the cobalt, which gives an estimation of chemisorbed CO of 12.6 $cm^3\,g^{-1}$ and 6.7 $cm^3\,g^{-1}$, respectively. These data gave further evidence of the high affinity of the materials for CO sorption and selectivity against N_2, O_2 and CO_2. Compared to the reported cobalt complexed POPs [22], the **2D-COF-CorCo** presented a 3.2 and 1.3 fold greater selectivity for CO with respect to N_2 and O_2 and similar CO selectivity over CO_2. This 2D COF has shown a higher ratio of cobalt active site of 56.2 %, which could be assigned to the higher crystallinity and stability of the porous structure, as well as to the regularity and uniformity of the pore distribution. Furthermore, interpenetration of the framework often happens in 3D COFs [50, 76] which should reduce the porosity in the case of **3D-COF-CorCo**, and inhibits the accessibility of the cobalt sites and therefore the binding with CO molecules.

The selectivity for CO over O_2, N_2 and CO_2 was determined by IAST calculations according to the fitting parameters deduced from the multisite and single site Langmuir models, considering a gas mixture containing 100 ppm of CO in the other gases (Fig. 4c,d). These conditions were chosen to estimate the suitability of the materials for CO sensing in a real atmosphere, which is mainly composed by N_2, O_2 and CO_2. At zero pressure, the calculations gave very high selectivity values for CO over N_2 (50129 and 22691) and O_2 (5088 and 6800) for **2D** and **3D-COF-CorCo**, respectively. These values correspond to the ratio of their corresponding Henry constants at zero pressure. In all cases, the selectivities decrease gradually with increasing pressure, but still remain higher than 11000 over N_2 and 1400 over O_2 at 1 atm. Aside from the selectivity, **2D-COF-CorCo** showed the highest capacity for CO at low pressure ($P < 0.1$ atm) compared to either **3D-COF-CorCo** or the recently reported POPs based on cobalt corrole [22]. This result should be assigned to the better accessibility of the cobalt site in **2D-COF-CorCo**

for CO binding owing to the better structuration and organization of the pore channels. Accordingly, it is considered that the selectivity of **2D/3D-COF-CorCo** for CO over N_2, O_2 and CO_2 is far higher than those reported for other porous materials like MOFs and POPs [22, 77, 78]. Despite the lower selectivity for CO over CO_2 compared to other gases, the CO/CO_2 selectivity is still high (> 20) at 1 atm even with a CO/CO_2 ratio of 0.01/99.99. However, in a real atmosphere containing 400 ppm of CO_2, only the selectivities at low partial pressures of CO_2 must be considered for the targeted application as CO sensors. Furthermore, the reversibility of the materials for CO was studied by recording successive CO adsorption cycles after degassing at 80 °C between each sorption cycle (Fig. S32-S33). The results showed that after 4 cycles, both COFs gave satisfactory reversibility results. The slight decrease of CO adsorption between the first and forth cycle could be assigned to a partial collapse of the structures and porosities, as shown by the decrease of their BET surfaces after 4 cycles (Fig. 4a and S30).

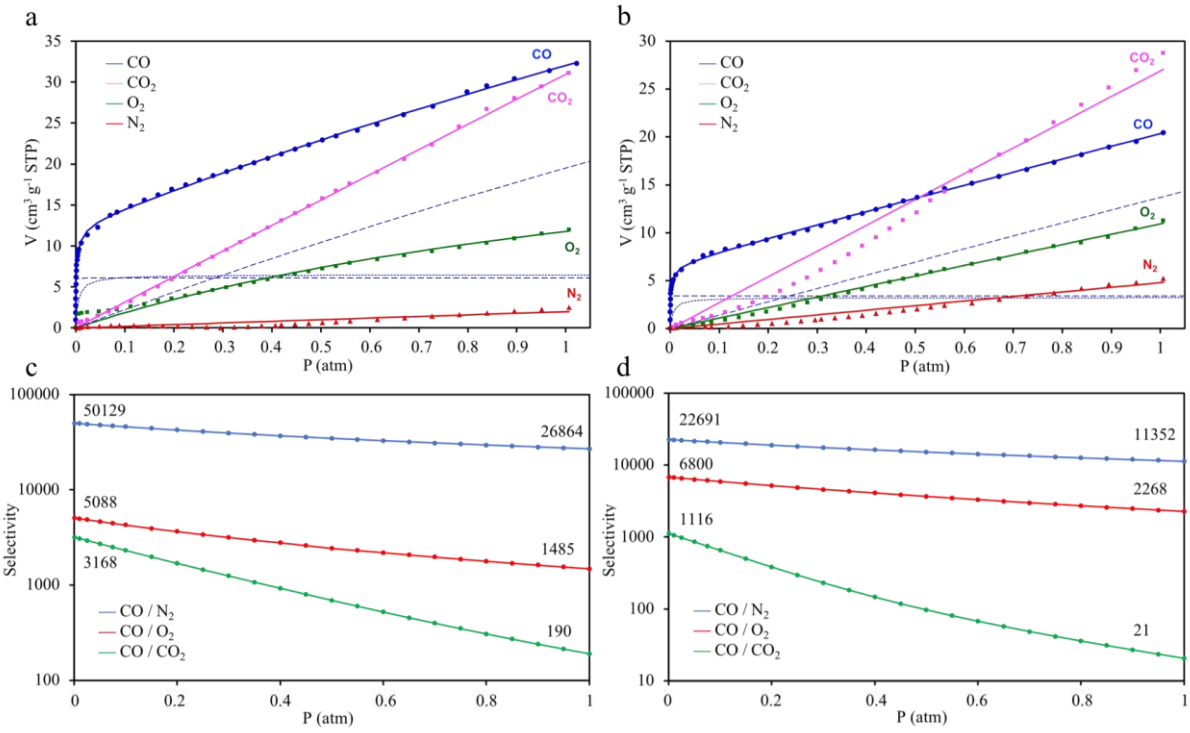

Fig. 4. Adsorption isotherms of CO (blue), CO_2 (pink), N_2 (red) and O_2 (green) recorded at 298 K for (a) **2D-COF-CorCo** and (b) **3D-COF-CorCo**. Solid lines represent fitting curves using a single-site Langmuir model for N_2, O_2 and CO_2, and a triple-site Langmuir model for CO. IAST selectivity calculations at 298 K for CO over CO_2, N_2 and O_2 for (c) **2D-COF-CorCo** and (d) **3D-COF-CorCo** assuming a 0.01: 99.99 mixture (100 ppm CO in N_2, O_2 or CO_2).

The reversibility study of the CO adsorption for **2D** and **3D-COF-CorCo** were also carried out by FTIR spectroscopy in transmission mode using KBr pellets of COFs under either a CO atmosphere or under vacuum (Fig. 5a,b) and Fig. S34-S37). Before exposure to CO, the activation of these materials was achieved under vacuum at 20 °C in order to remove the coordinated ammine on the cobalt corrole. After 24 h, the ammine ligands were removed since the characteristic stretching vibration of NH_3 totally vanished. Then, the KBr pellet was placed in a CO atmosphere (1 bar) for 1 h and the chamber was purged for 5 min with nitrogen to remove extra CO. For **2D-COF-CorCo**, an intense vibration band at 2044 cm^{-1} appeared and this frequency value is characteristic to CO bounded to a metal ion *via* the carbon atom [22]. The lower value compared to free CO (2143 cm^{-1}) is assigned to the sigma donation of CO from the carbon orbital into the empty d_{z2} orbital of cobalt. The electron density can also be π-back donated from d orbitals of the cobalt to π-antibonding orbitals of CO [79-81]. This π-backdonation tends to weaken the CO bond vibration leading to a red-shift of the CO stretching frequency with respect to free CO (2143 cm^{-1}), as already observed in a Co(III) corrole series [20, 22].

Successive spectra were then recorded after exposure the chamber to vacuum (2 mbar). As displayed in Fig. 5b, a constant decrease of the bonded CO vibration intensity was observed over time under vacuum. After 90 h, the CO vibration almost disappeared and the intensity did not change any more, which means that there was no more CO coordinated on cobalt corroles. However, the half-desorption time was rather short since it was estimated to 30 min (Fig. S36). These data clearly reveal that CO adsorption in the COFs involved the coordination of the gaseous molecules on the cobalt atom according to a reversible process. For **3D-COF-CorCo**, similar results for the reversible process were observed (Fig. S34 and S37). The only difference is that it took only 36 h to remove all the bonded CO to the cobalt corroles. However, both of them showed a fast CO desorption in the first hour which indicated a fast and reversible CO desorption.

The reversibility for CO binding on **2D** and **3D-COF-CorCo** was studied by carrying out two cycles of adsorption and desorption of CO, and monitored by FTIR. For **2D-COF-CorCo**, after 80 h vacuum, the CO was desorbed until it reached an equilibrium but it did not desorb completely (Fig. S36). This could be caused by the π-stacking structure of 2D COF, which makes it more difficult to release CO. For **3D-COF-CorCo**, the first cycle of sorption and desorption of CO presented the same behavior as for 2D-COF-CorCo. However, for the second

cycle the desorption of CO was total (Fig. S37). These results showed good reversibility of CO binding and desorption for **2D** and **3D-COF-CorCo**.

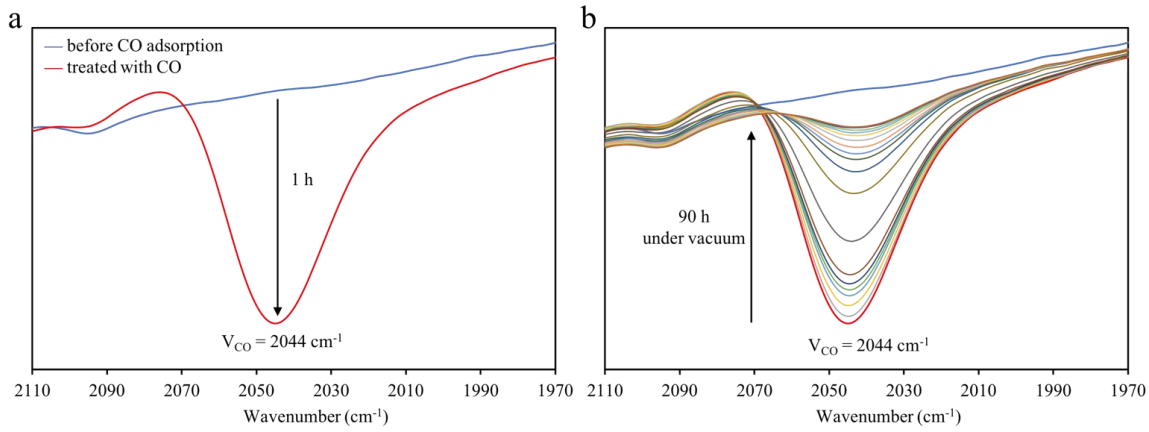

Fig. 5. FTIR monitoring of the adsorption/desorption process recorded for **2D-COF-CorCo**: (a) activated **2D-COF-CorCo** and treated with CO for 1 h, (b) during desorption under vacuum (1 min to 90 h)

3. Conclusion

In summary, we report for the first time novel corrole-based 2D and 3D COFs *via* imine condensation reaction using C_2 symmetric corrole linker. The resulted porous **2D-COF-Cor** showed good crystallinity with a hexagonal packing. Interestingly, the crystallinity and permanent porosity were preserved after post-metalation with cobalt. In contrast, three dimensional **3D-COF-Cor** showed a microporous but amorphous structure. Both corrole-based materials also show a high surface area that reached 1266 m^2 g^{-1} in the case of the 2D COF. In contrast, 3D COF showed a lower BET surface area of 416 m^2 g^{-1}. Post-metalation allowed us to insert cobalt into the corrole macrocycle almost quantitatively in order to obtain the targeted COFs-CorCo for further CO adsorption. Both of them exhibited outstanding affinities and selectivities for CO binding over N_2, O_2 and CO_2. It is also worth noting that the adsorption of CO for COFs-Co is reversible through at least 4 cycles, even if a slight decrease of CO uptake was observed. However, the CO adsorption for both COFs tend to be stable after 4 cycles since it did not decrease anymore after 4 cycles. We have also shown that the combination of crystallinity and regular porosity of the framework allow a better accessibility of the cobalt corrole for gas binding. Desorption of CO was studied by FTIR that show that both COFs exhibit a fast desorption of CO with a half-desorption time estimated to 30 min. This result is a

real prerequisite to build sensors with fast response. These results demonstrate that the combination of cobalt corroles and COF materials provides an attractive strategy for the selective CO capture, and our work are currently in progress for developing new gas sensor technologies featuring great potential of applications.

Authors Contributions

Jian Yang: Methodology, synthesis, characterization, analysis, writing.

Laurie André: Methodology, characterization, writing, review and editing.

Claude P. Gros: Supervision, review, editing, and project administration.

Nicolas Desbois: Supervision of the corroles synthesis, review, editing.

Stéphane Brandès: Conceptualization, methodology, analysis, writing, review and editing.

Declaration of competing interest

The authors declare no competing interest.

Data availability

The raw/processed data required to reproduce these findings cannot be shared at this time due to technical or time limitations.

Acknowledgements

This work was supported by the CNRS (UMR UB-CNRS 6302, the "*Université Bourgogne Franche-Comté* (UBFC)", and the "*Conseil Régional de Bourgogne*" through the Plan d'Actions Régional pour l'Innovation (PARI II CDEA) and the European Union through the PO FEDER-FSE Bourgogne 2014/2020 (*via* the CoMICS program, Chemistry of Molecular Interactions: Catalysis & Sensors and the ISITE CO2DECIN). The French Research Agency (ANR) is also greatly acknowledged for financial support (AAPG 2015, ANR-15-CE04-0008, CO3SENS project) and the ISITE CO2DECIN (ANR-15-IDEX-0003, UBFC). JY thanks the French Ministry of Research (MESRI) for a PhD grant. The authors wish also to warmly thank Mrs Sandrine Pacquelet for technical assistance and the "*Plateforme d'Analyse Chimique et de Synthèse Moléculaire de l'Université de Bourgogne*" (SATT SAYENS, PACSMUB, http://www.wpcm.fr) for access to spectroscopy instrumentation (NMR, IR, ESI and MALDI/TOF LRMS and ESI HRMS). The authors thank Dr. Quentin Bonnin and Mrs. Marie-José Penouilh (University of Burgundy, PACSMUB) for HRMS analysis and Dr. Myriam Heydel for ICP analysis. The authors wish also to thank DImaCell Imaging Center

facilities (INRAE, *Université Bourgogne Franche-Comté*) and especially the expertise of Mrs. Aline Bonnotte for conducting the experiments on CRYO-SEM and EDS. We would also like to thank "*Applications, Recherches et Caractérisations à l'Echelle Nanométrique*" (ARCEN, *Laboratoire Interdisciplinaire Carnot de Bourgogne*) and especially Dr. Cédric Thomas for conducting the experiments for the SEM analysis.

Appendix A. Supplementary data

Supplementary data to this article can be found online at:

References

[1] H. Kinoshita, H. Türkan, S. Vucinic, et al., Carbon monoxide poisoning, Toxicol. Rep., 7 (2020) 169-173.

[2] M. Calik, T. Sick, M. Dogru, et al., From highly crystalline to outer surface-functionalized Covalent Organic Frameworks-A modulation approach, J. Am. Chem. Soc., 138 (2016) 1234-1239.

[3] S. Dey, G.C. Dhal, Materials progress in the control of CO and CO_2 emission at ambient conditions: An overview, Mater. Sci. Energy Technol., 2 (2019) 607-623.

[4] W. Zhang, F. Yang, J. Xu, C. Gu, et al.,Sensitive carbon monoxide gas sensor based on chemiluminescence on nano-Au/Nd_2O_3-$Ca_3Nd_2O_6$: working condition optimization by response surface methodology, ACS Omega, 5 (2020) 20034-20041.

[5] T. Nandy, R.A. Coutu, C. Ababei, Carbon monoxide sensing technologies for next-generation cyber-physical systems, Sensors, 18 (2018) 3443.

[6] J. Zuo, S. Tavakoli, D. Mathavakrishnan, et al., Additive manufacturing of a flexible carbon monoxide sensor based on a SnO_2-graphene nanoink, Chemosensors, 8 (2020) 36.

[7] A.M. Pineda-Reyes, M.R. Herrera-Rivera, H. Rojas-Chávez, et al., Recent advances in ZnO-based carbon monoxide sensors: role of doping, Sensors, 21 (2021) 4425.

[8] Y. Sun, Z. Zhao, K. Suematsu, et al., Rapid and stable detection of carbon monoxide in changing humidity atmospheres using clustered In_2O_3/CuO nanospheres, ACS Sensors, 5 (2020) 1040-1049.

[9] U.T. Nakate, P. Patil, S.-I. Na, et al., Fabrication and enhanced carbon monoxide gas sensing performance of p-CuO/n-TiO_2 heterojunction device, Colloids Surf. A. Physicochem., 612 (2021) 125962.

[10] D. Majumder, S. Roy, Development of low-ppm CO Sensors using pristine CeO_2 nanospheres with high surface area, ACS Omega, 3 (2018) 4433-4440.

[11] A.K. Basu, P.S. Chauhan, M. Awasthi, et al., α-Fe_2O_3 loaded rGO nanosheets based fast response/recovery CO gas sensor at room temperature, Appl. Surf. Sci., 465 (2019) 56-66.

[12] Y.S. Haiduk, A.A. Khort, N.M. Lapchuk, et al., Study of WO_3-In_2O_3 nanocomposites for highly sensitive CO and NO_2 gas sensors, J. Solid State Chem., 273 (2019) 25-31.

[13] F.M. Othman, A.A.A. Hamead, M.H.A. Wahid, Fabrication and characterization of CdO gas sensor with tube shape, Mater. Sci. Forum, 1021 (2021) 317-326.

[14] R. Molavi, M.H. Sheikhi, Facile wet chemical synthesis of Al doped CuO nanoleaves for carbon monoxide gas sensor applications, Mater. Sci. Semicond Process, 106 (2020) 104767.

[15] C. Cheng, C. Zhang, X. Gao, et al., 3D Network and 2D paper of reduced graphene oxide/Cu_2O composite for electrochemical sensing of hydrogen peroxide, Anal. Chem., 90 (2018) 1983-1991.

[16] R.J. Isaifan, M. Couillard, E.A. Baranova, Low temperature-high selectivity carbon monoxide methanation over yttria-stabilized zirconia-supported Pt nanoparticles, Int. J. Hydrog. Energy, 42 (2017) 13754-13762.

[17] A. Burresi, A. Fort, S. Rocchi, et al., Dynamic CO recognition in presence of interfering gases by using one MOX sensor and a selected temperature profile, Sens. Actuators, B, 106 (2005) 40-43.

[18] F. Rock, N. Barsan, U. Weimar, Electronic nose: current status and future trends, Chem. Rev., 108 (2008) 705-725.

[19] X. Zhou, S. Lee, Z. Xu, J. Yoon, Recent progress on the development of chemosensors for gases, Chem. Rev., 115 (2015) 7944-8000.

[20] J.-M. Barbe, G. Canard, S. Brandès, et al., Metallocorroles as sensing components for gas sensors: remarkable affinity and selectivity of cobalt(III) corroles for CO *vs.* O_2 and N_2, Dalton Trans., (2004) 1208-1214.

[21] J.-M. Barbe, G. Canard, S. Brandès, R. Guilard, Selective chemisorption of carbon monoxide by organic-inorganic hybrid materials incorporating Cobalt(III) corroles as sensing components, Chem. Eur. J. 13 (2007) 2118-2129.

[22] S. Brandès, V. Quesneau, O. Fonquernie, et al., Porous Organic Polymers based on cobalt corroles for carbon monoxide binding, Dalton Trans., 48 (2019) 11651-11662.

[23] C. Di Natale, C.P. Gros, R. Paolesse, Corroles at work: a small macrocycle for great applications, Chem. Soc. Rev., 51 (2022) 1277-1335.

[24] C.M. Lemon, P.J. Brothers, The synthesis, reactivity, and peripheral functionalization of corroles, J. Porphyr. Phthalocyanines, 15 (2011) 809-834.

[25] F. Wu, J. Xu, H. Gao, et al., A cationic benzocorrole Cu(II) complex as a highly stable antiaromatic system, Chem. Commun., 57 (2021) 383-386.

[26] S. Mondal, P.K. Naik, J.K. Adha, et al., Synthesis, characterization, and reactivities of high valent metal–corrole (M = Cr, Mn, and Fe) complexes, Coord. Chem. Rev., 400 (2019) 213043.

[27] Y. Li, M. Chen, Y. Han, et al., Fabrication of a new corrole-based Covalent Organic Framework as a highly efficient and selective chemosensor for heavy metal ions, Chem. Mater., 32 (2020) 2532-2540.

[28] J. Herritsch, J.-N. Luy, S. Rohlf, et al., Influence of ring contraction on the electronic structure of nickel tetrapyrrole complexes: corrole *vs* porphyrin, ECS J. Solid State SciTechnol., 9 (2020) 061005.

[29] M. Vanotti, S. Poisson, V. Soumann, et al., Influence of interfering gases on a carbon monoxide differential sensor based on SAW devices functionalized with cobalt and copper corroles, Sens. Actuators, B, 332 (2021) 129507.

[30] C. Li, J. Yang, P. Pachfule, et al., Ultralight Covalent Organic Framework/graphene aerogels with hierarchical porosity, Nat. Commun., 11 (2020) 4712.

[31] D. Rodríguez-San-Miguel, C. Montoro, F. Zamora, Covalent Organic Framework nanosheets: preparation, properties and applications, Chem. Soc. Rev., 49 (2020) 2291-2302.

[32] S. Dalapati, S. Jin, J. Gao, et al., An azine-linked Covalent Organic Framework, J. Am. Chem. Soc., 135 (2013) 17310-17313.

[33] X. Feng, X. Ding, D. Jiang, Covalent Organic Frameworks, Chem. Soc. Rev., 41 (2012) 6010-6022.

[34] H.-C. Ma, J. Zou, X.-T. Li, et al., Frontispiece: homochiral Covalent Organic Frameworks for asymmetric catalysis, Chem. Eur. J. 26 (2020).

[35] Austin M. Evans, M.R. Ryder, et al., Trends in the thermal stability of two-dimensional Covalent Organic Frameworks, Faraday Discuss., 225 (2021) 226-240.

[36] H. Wang, H. Wang, Z. Wang, et al., Covalent Organic Framework photocatalysts: structures and applications, Chem. Soc. Rev., 49 (2020) 4135-4165.

[37] L. Wang, C. Zeng, H. Xu, et al., A highly soluble, crystalline Covalent Organic Framework compatible with device implementation, Chem. Sci., 10 (2019) 1023-1028.

[38] H.-L. Qian, C. Dai, C.-X. Yang, et al., High-crystallinity Covalent Organic Framework with dual fluorescence emissions and its ratiometric sensing application, ACS Appl. Mater. Interfaces, 9 (2017) 24999-25005.

[39] G. Zhou, Z. Du, Y. Ma, et al., Molecular simulation study on gas adsorption and separation performance of alkyl-functionalized HKUST materials, Comput. Mater. Sci., 181 (2020) 109755.

[40] S. Liu, W.-L. Li, J.-P. Zhang, Revealing the potential application of chiral Covalent Organic Frameworks in CO_2 adsorption and separation, New. J. Chem., 44 (2020) 95-101.

[41] Y. Li, J. Zhang, K. Zuo, et al., Covalent Organic Frameworks for simultaneous CO_2 capture and selective catalytic transformation, Catalysts, 11 (2021) 1133.

[42] J. Guo, D. Jiang, Covalent Organic Frameworks for heterogeneous catalysis: principle, current status, and challenges, ACS Cent. Sci., 6 (2020) 869-879.

[43] D.-M. Li, S.-Q. Li, J.-Y. Huang, et al., A recyclable bipyridine-containing Covalent Organic Framework-based QCM sensor for detection of Hg(II) ion in aqueous solution, J. Solid State Chem., 302 (2021) 122421.

[44] S. Chen, B. Yuan, G. Liu, et al., Electrochemical sensors based on Covalent Organic Frameworks: a critical review, Front. Chem., 8 (2020).

[45] X. Ren, G. Liao, Z. Li, et al., Two-dimensional MOF and COF nanosheets for next-generation optoelectronic applications, Coord. Chem. Rev., 435 (2021) 213781.

[46] N. Keller, T. Bein, Optoelectronic processes in Covalent Organic Frameworks, Chem. Soc. Rev., 50 (2021) 1813-1845.

[47] D.-G. Wang, T. Qiu, W. Guo, et al., Covalent Organic Framework-based materials for energy applications, Energy Environ. Sci., 14 (2021) 688-728.

[48] B.C. Patra, S. Bhattacharya, New covalent organic square lattice based on porphyrin and tetraphenyl ethylene building blocks toward high-performance supercapacitive energy storage, Chem. Mater., 33 (2021) 8512-8523.

[49] N. Huang, P. Wang, D. Jiang, Covalent Organic Frameworks: a materials platform for structural and functional designs, Nat. Rev. Mater., 1 (2016) 16068.

[50] Y. Meng, Y. Luo, J.L. Shi, et al., 2D and 3D porphyrinic Covalent Organic Frameworks: The influence of dimensionality on functionality, Angew. Chem. Int. Ed., 59 (2020) 3624-3629.

[51] J. Guo, Y. Xu, S. Jin, et al., Conjugated organic framework with three-dimensionally ordered stable structure and delocalized π clouds, Nat. Commun., 4 (2013) 2736.

[52] D. Kaleeswaran, P. Vishnoi, R. Murugavel, [3+3] Imine and β-ketoenamine tethered fluorescent Covalent-Organic Frameworks for CO_2 uptake and nitroaromatic sensing, J. Mater. Chem. C, 3 (2015) 7159-7171.

[53] H. Ding, J. Li, G. Xie, et al., An AIEgen-based 3D Covalent Organic Framework for white light-emitting diodes, Nat. Commun., 9 (2018) 5234.

[54] S.J. Lyle, P.J. Waller, O.M. Yaghi, Covalent Organic Frameworks: organic chemistry extended into two and three dimensions, Trends Chem., 1 (2019) 172-184.

[55] K. Geng, T. He, R. Liu, et al., Covalent Organic Frameworks: design, synthesis, and functions, Chem. Rev., 120 (2020) 8814-8933.

[56] R.R. Liang, S.Y. Jiang, R.H. A, et al., Two-dimensional Covalent Organic Frameworks with hierarchical porosity, Chem. Soc. Rev., 49 (2020) 3920-3951.

[57] X. Guan, F. Chen, Q. Fang, et al., Design and applications of three dimensional Covalent Organic Frameworks, Chem. Soc. Rev., 49 (2020) 1357-1384.

[58] S. Wu, Y. Pan, H. Lin, et al., Crystalline Covalent Organic Frameworks with tailored linkages for photocatalytic H_2 evolution, ChemSusChem, 14 (2021) 4958-4972.

[59] R. Liu, K.T. Tan, Y. Gong, et al., Covalent Organic Frameworks: an ideal platform for designing ordered materials and advanced applications, Chem. Soc. Rev., 50 (2021) 120-242.

[60] Y. Zhao, W. Dai, Y. Peng, et al., A corrole-based Covalent Organic Framework featuring desymmetrized topology, Angew. Chem. Int. Ed., 59 (2020) 4354-4359.

[61] S. Kandambeth, K. Dey, R. Banerjee, Covalent Organic Frameworks: chemistry beyond the structure, J. Am. Chem. Soc., 141 (2019) 1807-1822.

[62] A. Jiménez-Almarza, A. López-Magano, L. Marzo, et al., Imine-based Covalent Organic Frameworks as photocatalysts for metal free oxidation processes under visible light conditions, ChemCatChem, 11 (2019) 4916-4922.

[63] Z.-C. Guo, Z.-Q. Shi, X.-Y. Wang, et al., Proton conductive Covalent Organic Frameworks, Coord. Chem. Rev., 422 (2020) 213465.

[64] X. Ma, T.F. Scott, Approaches and challenges in the synthesis of three-dimensional covalent-organic frameworks, Commun. Chem., 1 (2018) 98.

[65] J.K. Laha, S. Dhanalekshmi, M. Taniguchi, et al., A scalable synthesis of *meso*-substituted dipyrromethanes, Org. Process. Res. Dev., 7 (2003) 799-812.

[66] S. Yan, X. Guan, H. Li, et al., Three-dimensional salphen-based Covalent–Organic Frameworks as catalytic antioxidants, J. Am. Chem. Soc., 141 (2019) 2920-2924.

[67] L. Zeng, P. Liao, H. Liu, et al., Impregnation of metal ions into porphyrin-based imine gels to modulate guest uptake and to assemble a catalytic microfluidic reactor, J. Mater. Chem. A, 4 (2016) 8328-8336.

[68] G. Lin, H. Ding, R. Chen, et al., 3D Porphyrin-based Covalent Organic Frameworks, J. Am. Chem. Soc., 139 (2017) 8705-8709.

[69] V. Quesneau, W. Shan, N. Desbois, et al., Cobalt corroles with bis-ammonia or mono-DMSO axial ligands. Electrochemical, spectroscopic characterizations and ligand binding properties, Eur. J. Inorg. Chem. (2018) 4265-4277.

[70] N.I. Neuman, A. Singha Hazari, J. Beerhues, et al., Synthesis and characterization of a Cobalt(III) corrole with an S-Bound DMSO ligand, Eur. J. Inorg. Chem. (2021) 3540-3548.

[71] D. Zhu, Y. Zhu, Q. Yan, et al., Pure crystalline Covalent Organic Framework aerogels, Chem. Mater., 33 (2021) 4216-4224.

[72] Z. Zhao, D. Zheng, M. Guo, et al., Engineering olefin-linked Covalent Organic Frameworks for photoenzymatic reduction of CO_2, Angew. Chem. Int. Ed., 61 (2022) e202200261.

[73] J. Hynek, J. Zelenka, J. Rathouský, et al., Designing porphyrinic Covalent Organic Frameworks for the photodynamic inactivation of bacteria, ACS Appl. Mater. Interfaces, 10 (2018) 8527-8535.

[74] J. Rouquerol, P. Llewellyn, F. Rouquerol, Is BET equation applicable to microporous adsorbents?, Stud. Surf. Sci. Catal., 160 (2007) 49-56.

[75] Y. Zhao, Y. Peng, C. Shan, et al., Metallocorrole-based Porous Organic Polymers as a heterogeneous catalytic nanoplatform for efficient carbon dioxide conversion, Nano. Res., 15 (2021) 1145-1152.

[76] R.P. Bisbey, W.R. Dichtel, Covalent Organic Frameworks as a platform for multidimensional polymerization, ACS Cent. Sci., 3 (2017) 533-543.

[77] A. Evans, R. Luebke, C. Petit, The use of Metal–Organic Frameworks for CO purification, J. Mater. Chem. A, 6 (2018) 10570-10594.

[78] E.D. Bloch, M.R. Hudson, J.A. Mason, et al., Reversible CO binding enables tunable CO/H_2 and CO/N_2 separations in Metal-Organic Frameworks with exposed divalent metal cations, J. Am. Chem. Soc., 136 (2014) 10752-10761.

[79] G. Frenking, N. Fröhlich, The nature of the bonding in transition-metal compounds, Chem. Rev., 100 (2000) 717-774.

[80] M. Zhou, L. Andrews, C.W. Bauschlicher, Spectroscopic and theoretical investigations of vibrational frequencies in binary unsaturated transition-metal carbonyl cations, neutrals, and anions, Chem. Rev., 101 (2001) 1931-1962.

[81] X. Wu, L. Zhao, D. Jiang, et al., Barium as honorary transition metal in action: experimental and theoretical study of $Ba(CO)^+$ and $Ba(CO)^-$, Angew. Chem. Int. Ed., 57 (2018) 3974-3980.

Graphical Abstract